Robust Landing using Time-To-Collision Measurement with Actuator Saturation

Yoshiaki Kuwata[a] and Larry Matthies[a]

[a]Jet Propulsion Laboratory, California Institute of Technology,
4800 Oak Grove Drive, Pasadena, USA

ABSTRACT

This paper considers a landing problem for an MAV that uses only a monocular camera for guidance. Although this sensor cannot measure the absolute distance to the target, by using optical flow algorithms, time-to-collision to the target is obtained. Existing work has applied a simple proportional feedback control to simple dynamics and demonstrated its potential. However, due to the singularity in the time-to-collision measurement around the target, this feedback could require an infinite control action. This paper extends the approach into nonlinear dynamics. In particular, we explicitly consider the saturation of the actuator and include the effect of the aerial drag. It is shown that the convergence to the target is guaranteed from a set of initial conditions, and the boundaries of such initial conditions in the state space are numerically obtained. The paper then introduces parametric uncertainties in the vehicle model and in the time-to-collision measurements. Using an argument similar to the nominal case, the robust convergence to the target is proven, but the region of attraction is shown to shrink due to the existence of uncertainties. The numerical simulation validates these theoretical results.

Keywords: Time-to-collision, Convergence, Actuator saturation, Parametric uncertainty

1. INTRODUCTION

Micro Aerial Vehicles (MAVs) is an enabling technology for wide variety of military and civilian missions especially in cluttered and/or urban environments, because of their high manoeuvrability, small size, and easy deployment.[1] One important mission is a surveyance of an area, in which the ability to "perch and stare" can save the limited onboard power resources. To perform such mission successfully, MAVs must have an auto-landing capability.

Due to their size, MAVs can carry small payload or sensors, which makes the landing problem different from the conventional aircraft landing that can use various sensors such as GPS, IMU, altimeter, radar, as well as the prior maps of the landing area. Inspired by the studies on biological systems such as insects[2] or small birds,[3] this paper considers a monocular camera as the only guidance sensor[4] for the landing task. When landing on a flat surface, a monocular camera can provide the angular velocity V_f/h of the image of the ground. Bees have been shown to hold this angular velocity constant while descending, which makes the horizontal speed decrease linearly with respect to the height, resulting in a smooth landing.[2]

When landing on a target point, the primary challenge with a monocular camera is that it can estimate the vehicle speed and distance only up to a scale factor, without the aid of other sensors.[5] However, a time-to-collision (TTC) to the target can be obtained by running optical flow algorithms on the obtained images,[6–10] even with a rotational egomotion.[10] Using this TTC, several landing algorithms have been proposed in the past, such as keeping the derivative of TTC constant[3] (which could be potentially very noisy) and keeping TTC constant.[2,10,11] Using a proportional controller, vertical landing onto a surface using TTC has been experimentally demonstrated,[10–12] but, no analysis has been done when the vehicle model has nonlinearities such as control saturation and air drag, and uncertainties in the measurements and/or modeling parameters. With the saturation, the widely used proportional controller does not lead to globally asymptotic stability of the closed-loop system. However, this paper shows the convergence to the target is guaranteed from a set of initial conditions and that the boundary of region of attraction is numerically computed.

Further author information: (Send correspondence to Yoshiaki Kuwata)
Yoshiaki Kuwata: E-mail: Yoshiaki.Kuwata@jpl.nasa.gov, Telephone: 1 818 245 2717
Larry Matthies: E-mail: lhm@jpl.nasa.gov, Telephone: 1 818 354 3722

The rest of the paper is organized as follows. Following the problem statement in Section 2, Section 3 gives a control law. Section 4 provides theoretical and numerical analysis of the controller. Then, Section 5 investigates how the system behaves under the uncertainties in the measurement and modeling errors. Finally, Section 6 shows numerical simulation results.

2. PROBLEM STATEMENT

This paper considers the along-track motion of the UAV landing on a particular target point on a flat surface. The vehicle model is given by

$$m\ddot{r} = u - \mathrm{sgn}(\dot{r})\frac{1}{2}\rho\dot{r}^2 C_d A$$

where m is the vehicle mass, r is the distance to the target, u is the control input, ρ is the air density, C_d is the drag coefficient, and A is the projected frontal area. The control input has saturation limits

$$|u| \le u_{\max}.$$

Without loss of generality, the target is assumed to be at the origin $r = 0$. The vehicle is assumed to start at $r = r_0$, where $r_0 > 0$. The region with $r < 0$ is considered to be a wall or a no-fly zone that the vehicle should not enter.

The time-to-collision (TTC) to the target is obtained by running optical flow algorithms and computing the divergence of the flow field. In this paper, we focus on the controller analysis and do not give the details of the optical flow algorithm (see references[8–10]). The TTC

$$\mathrm{TTC} = -\frac{r}{\dot{r}} \tag{1}$$

is estimated and is assumed to be given to the controller. To land on the target successfully, the vehicle must come sufficiently close to the target while slowing down below some threshold. Let $\mathscr{G}$ denote such target set in the phase plane

$$\mathscr{G} = \left\{(r,\dot{r}) \mid 0 \le r \le r_f,\ v_f \le \dot{r} \le 0\right\} \tag{2}$$

Here, the paper assumes that once the vehicle enters this set, some latching mechanism (equivalent of the "legs" of the insects) ensures the successful landing.

To simplify the presentation, let m be set to be 1, and introduce a parameter $\alpha \doteq \frac{1}{2}\rho C_d A$. Then, the system is represented as

$$\frac{d}{dt}\begin{bmatrix} r \\ \dot{r} \end{bmatrix} = \begin{bmatrix} \dot{r} \\ u - \mathrm{sgn}(\dot{r})\alpha\dot{r}^2 \end{bmatrix}. \tag{3}$$

3. CONTROL LAW

Note that if TTC is constant, from Eq. (1) both the distance r and the speed $\dot{r}$ exponentially converge to 0.[2] Motivated by this observation, the control law to be considered has a form

$$\begin{aligned} u &= K(c - \mathrm{TTC}) \\ &= K\left(c + \frac{r}{\dot{r}}\right) \end{aligned}$$

when TTC is positive.[10,11] The parameters K and c are selected by the control designer. When TTC is negative, the vehicle is heading away from the target, and $u = -u_{\max}$ should be applied. In order to account also for the limits on the control input, the proposed control law is written as

$$u = \begin{cases} -u_{\max} & \text{if } r \ge \dot{r}\left(-\frac{u_{\max}}{K} - c\right) \\ u_{\max} & \text{else if } r < \dot{r}\left(\frac{u_{\max}}{K} - c\right) \\ K\left(c + \frac{r}{\dot{r}}\right) & \text{otherwise} \end{cases} \tag{4}$$

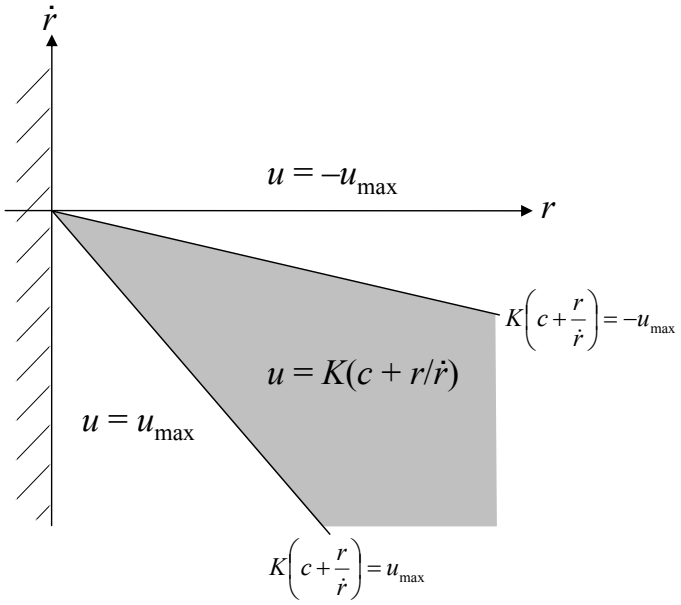

Figure 1. Control law in the phase plane

Figure 1 gives this control law in the phase plane. Note that when $\dot{r} < 0$, Eq. (4) can be written as

$$u = u_{\max} \operatorname{sat}\left(\frac{K}{u_{\max}}\left(c + \frac{r}{\dot{r}}\right)\right) \tag{5}$$

where the saturation function is defined as

$$\operatorname{sat}(x) = \begin{cases} x & \text{if } |x| \geq 1 \\ \operatorname{sgn}(x) & \text{otherwise.} \end{cases}$$

4. CONTROLLER ANALYSIS

This section analyzes the closed-loop behavior of the control law and the system in Section 3.

LEMMA 4.1. *The system* Eq. (3) *controlled by* Eq. (4) *does not have equilibrium states in* $r \geq 0$.

Proof. The proof is by contradiction. Assume the system Eq. (3) has an equilibrium. Then, the first row of Eq. (3) gives $\dot{r} = 0$. Combining this with the second row gives $u = 0$. However, from Eq. (4) $\dot{r} = 0$ in $r \geq 0$ means $u = -u_{\max}$, which is a contradiction. □

LEMMA 4.2. *The system* Eq. (3) *controlled by* Eq. (4) *does not become* $\dot{r} = 0$ *and* $r > 0$*, once* $\dot{r} < 0$ *and* $r > 0$.

Proof. It is sufficient to show that $\ddot{r}$ is strictly negative when $\dot{r}$ is negative and close to 0.

Consider the states that satisfy the following two conditions.

$$-\frac{r}{\frac{u_{\max}}{K} + c} < \dot{r} < 0 \tag{6}$$

$$-\sqrt{\frac{u_{\max}}{\alpha}} < \dot{r} < 0 \tag{7}$$

The condition Eq. (6), the control law Eq. (4), and the system equation Eq. (3) produce

$$\ddot{r} = -u_{\max} + \alpha \dot{r}^2.$$

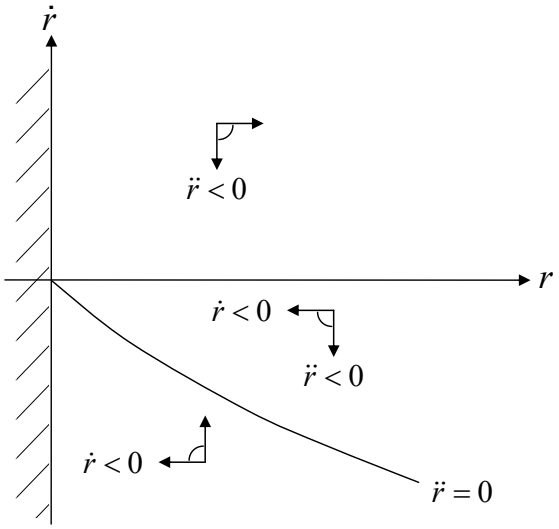

Figure 2. Direction of the trajectory in the phase plane. The line that corresponds to $\ddot{r} = 0$ is also shown.

Combining with Eq. (7), we have $\ddot{r} < 0$. □

THEOREM 4.3 (REACHING $r = 0$). *From any initial condition $x = [r_0, v_0]^T$ with $r_0 > 0$, the system* Eq. (3) *controlled by the control law* Eq. (4) *will reach $r = 0$.*

Proof. When $\dot{r} \geq 0$ and $r > 0$, it can be seen from Eq. (4) that $u = -u_{\max}$. Thus, $\ddot{r} < -u_{\max}$, and $\dot{r}$ becomes negative in finite time (at most in $v_0/u_{\max}$).

Once the vehicle states are in $r > 0$ and $\dot{r} < 0$, by Lemma 4.2 $\dot{r}$ remains negative, and hence the distance r decreases monotonically. From Lemma 4.1, there is no equilibrium in $r > 0$ with $\dot{r} = 0$, so that the system eventually reaches $r = 0$. □

The graphical representation of this theorem is shown in Figure 2.

Theorem 4.3 showed that the vehicle hits the target from any initial condition with $r_0 > 0$. The next theorem states that from a particular set of initial conditions the system enters the target set $\mathscr{G}$ defined in Eq. (2) with an appropriate velocity.

We first find a state trajectory of a closed-loop system Eq. (3) and Eq. (4), starting from the target $r = 0$ with a positive speed $v_0 > 0$ and ending at $r = 0$ and $\dot{r} = v_f$. This trajectory, denoted by l, can be obtained using any method such as bi-section search over v_0 and backward numerical integration. If l does not exist, we terminate. Otherwise, let $\mathscr{D}$ denote a region in the phase plane that is encircled by l and $r = 0$, but is outside of the target set $\mathscr{G}$.

THEOREM 4.4 (CONVERGENCE TO THE TARGET SET). *From any states in $\mathscr{D}$, the system* Eq. (3) *controlled by the control law* Eq. (4) *will enter $\mathscr{G}$.*

Proof. Let $\partial\mathscr{D}$ denote the boundary of $\mathscr{D}$. As illustrated in Figure 3, $\partial\mathscr{D}$ consists of three boundaries: $\partial\mathscr{D}_l$ along the trajectory l; $\partial\mathscr{D}_\mathscr{G}$ around the the target set $\mathscr{G}$; and $\partial\mathscr{D}_0$ at $r = 0$ with $\dot{r} > 0$.

From any states in $\mathscr{D}$, the system reaches $\partial\mathscr{D}$, because the system is going to reach $r = 0$ by Theorem 4.3. When the states reach $\partial\mathscr{D}_l$, the closed-loop system follows the trajectory l, which enters $\mathscr{G}$ by the definition of l. When the states reach $\partial\mathscr{D}_\mathscr{G}$, the system is in $\mathscr{G}$. When the system is on $\partial\mathscr{D}_0$ (but not on $\partial\mathscr{D}_\mathscr{G}$), because $\dot{r} > 0$ on $\partial\mathscr{D}_0$, the system leaves $\partial\mathscr{D}_0$ and eventually reaches either $\partial\mathscr{D}_\mathscr{G}$ or $\partial\mathscr{D}_l$.

□

From the argument above, the region $\mathscr{D}$ is the set of initial conditions from which the vehicle successfully reaches $\mathscr{G}$. The boundary $\partial\mathscr{D}_l$ can be obtained numerically, by integrating the system Eq. (3) and Eq. (4) backwards in time from $r = 0$, $\dot{r} = v_f$.

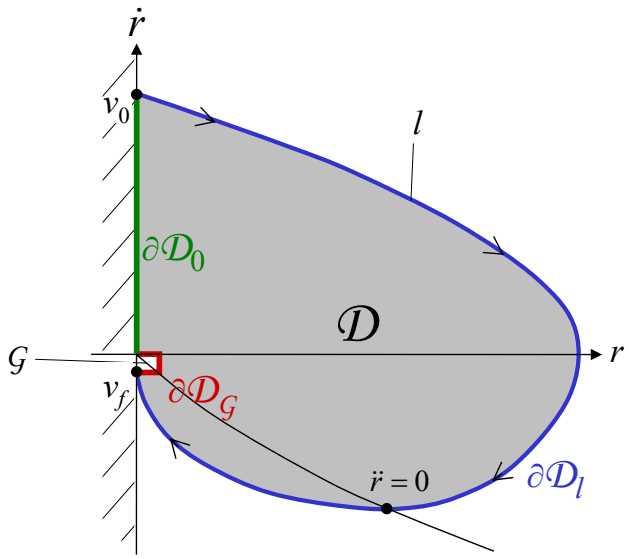

Figure 3. Region of attraction $\mathscr{D}$. The line of $\ddot{r}=0$ is also shown. Below this line, $\ddot{r}\geq 0$; above this line $\ddot{r}<0$.

5. EFFECT OF UNCERTAINTIES

This section investigates how the uncertainties in the parameters and measurements affect the behavior of the closed-loop system. We consider multiplicative bounded uncertainties on the TTC measurement $-\frac{r}{\dot{r}}$, controller input u, and the drag coefficient C_d. With the uncertainties, the system Eq. (3) becomes

$$\frac{d}{dt}\begin{bmatrix} r \\ \dot{r} \end{bmatrix} = \begin{bmatrix} \dot{r} \\ (1+\Delta_u)u - \mathrm{sgn}(\dot{r})(1+\Delta_\alpha)\alpha\dot{r}^2 \end{bmatrix} \tag{8}$$

where

$$u = \begin{cases} -u_{\max} & \text{if } (1+\Delta_m)r \geq \dot{r}\left(-\frac{u_{\max}}{K}-c\right) \\ u_{\max} & \text{else if } (1+\Delta_m)r < \dot{r}\left(\frac{u_{\max}}{K}-c\right) \\ K\left(c+(1+\Delta_m)\frac{r}{\dot{r}}\right) & \text{otherwise} \end{cases} \tag{9}$$

where Δ_u, Δ_α, and Δ_m are uncertain parameters whose norms are bounded by known constants

$$\begin{aligned} |\Delta_u| &\leq \delta_u < 1 \\ |\Delta_\alpha| &\leq \delta_\alpha < 1 \\ |\Delta_m| &\leq \delta_m < 1. \end{aligned}$$

5.1 Effect of Δ_u

Let l_u denote a state trajectory, starting from the target $r=0$ with a positive speed $v_0>0$ and ending at $r=0$ and $\dot{r}=v_f$, of the nominal closed-loop system Eq. (3) with the control input $\tilde{u}$ with

$$\tilde{u} = \begin{cases} (1-\delta_u)u & \text{if } \dot{r}\geq 0 \\ (1+\delta_u)u & \text{else if } u<0 \\ (1-\delta_u)u & \text{otherwise} \end{cases} \tag{10}$$

where u is given in Eq. (4). Again, we assume that this l_u is found by any numerical technique.

Let $\mathscr{D}_u$ denote a region in the phase plane that is encircled by l_u and $r=0$, but is outside of the target set $\mathscr{G}$. Then, the following holds.

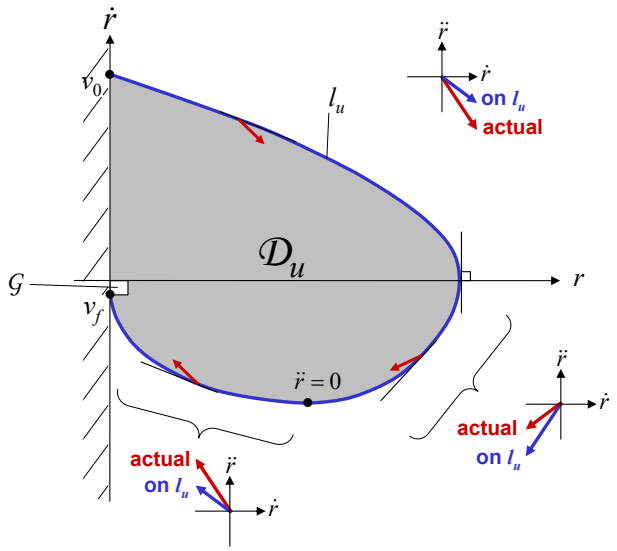

Figure 4. Region of attraction with uncertain gain on u.

THEOREM 5.1 (CONVERGENCE WITH AN UNCERTAIN GAIN). *From any states in $\mathscr{D}_u$, the system* Eq. (8) *with $\Delta_\alpha = 0$ controlled by the control law* Eq. (4) *will enter $\mathscr{G}$.*

Proof. The proof is based on investigating the instantaneous direction of the trajectory in the phase plane, given by $[\dot{r}, \ddot{r}]^T$, at the states on l_u. First, note that the trajectory l_u has an instantaneous direction $\left[\dot{r},\ \tilde{u} - \mathrm{sgn}(\dot{r})\alpha\dot{r}^2\right]^T$.

When $\dot{r} \geq 0$, then, $u < 0$ so that the actual system has

$$\begin{aligned}\ddot{r} &= (1+\Delta_u)u - \mathrm{sgn}(\dot{r})\alpha\dot{r}^2 \\ &\leq (1-\delta_u)u - \mathrm{sgn}(\dot{r})\alpha\dot{r}^2 \\ &= \tilde{u} - \mathrm{sgn}(\dot{r})\alpha\dot{r}^2\end{aligned}$$

so that the trajectory of the actual system goes more downward in the phase plane compared to l_u.

When $\dot{r} < 0$ and $u < 0$, the actual system has

$$\begin{aligned}\ddot{r} &= (1+\Delta_u)u - \mathrm{sgn}(\dot{r})\alpha\dot{r}^2 \\ &\geq (1+\delta_u)u - \mathrm{sgn}(\dot{r})\alpha\dot{r}^2 \\ &= \tilde{u} - \mathrm{sgn}(\dot{r})\alpha\dot{r}^2\end{aligned}$$

so that the trajectory of the actual system goes upwards compared to l_u.

When $\dot{r} < 0$ and $u \geq 0$, the actual system has

$$\begin{aligned}\ddot{r} &= (1+\Delta_u)u - \mathrm{sgn}(\dot{r})\alpha\dot{r}^2 \\ &\geq (1-\delta_u)u - \mathrm{sgn}(\dot{r})\alpha\dot{r}^2 \\ &= \tilde{u} - \mathrm{sgn}(\dot{r})\alpha\dot{r}^2\end{aligned}$$

so that the trajectory of the actual system goes upwards compared to l_u.

Figure 4 illustrates these cases. In any of these cases, any realizable trajectory on l_u goes inwards of $\mathscr{D}_u$. Because any trajectory inside $\mathscr{D}_u$ cannot cross l_u, using the same argument in the proof of Theorem 4.4, from any states in $\mathscr{D}_u$, the system Eq. (8) with $\Delta_\alpha = 0$ controlled by the control law Eq. (10) will enter $\mathscr{G}$.

□

5.2 Effect of Δ_α

Let l_α denote a state trajectory, starting from the target $r = 0$ with a positive speed $v_0 > 0$ and ending at $r = 0$ and $\dot{r} = v_f$, of a system

$$\ddot{r} = u - (1 - \delta_\alpha)\,\mathrm{sgn}(\dot{r})\alpha\dot{r}^2 \tag{11}$$

controlled by Eq. (4). Let $\mathscr{D}_\alpha$ denote a region in the phase plane that is encircled by l_α and $r = 0$, but is outside of the target set $\mathscr{G}$. Then, the following holds.

THEOREM 5.2 (CONVERGENCE WITH AN UNCERTAIN DRAG). *From any states in $\mathscr{D}_\alpha$, the system* Eq. (8) *with $\Delta_u = 0$ controlled by the control law* Eq. (4) *will enter $\mathscr{G}$.*

Proof. The proof is based on showing that any states on l_α of the actual system have a direction in the phase plane that goes inward of $\mathscr{D}_\alpha$.

Note that l_α has a slope of infinity when crossing $\dot{r} = 0$. Therefore, when $\dot{r} > 0$, if the actual system has $\ddot{r}$ that is smaller than that of l_α, the actual trajectory goes inward of $\mathscr{D}_\alpha$. Similarly, when $\dot{r} < 0$, if the actual system has $\ddot{r}$ that is larger than that of l_α, the actual trajectory goes inward of $\mathscr{D}_\alpha$.

At the states on l_α with $\dot{r} \geq 0$, the real system has

$$\begin{aligned}\ddot{r} &= u - (1 + \Delta_\alpha)\,\mathrm{sgn}(\dot{r})\alpha\dot{r}^2 \\ &\leq u - (1 - \delta_\alpha)\,\mathrm{sgn}(\dot{r})\alpha\dot{r}^2\end{aligned}$$

so that the real system goes more downward than l_α. At the states on l_α with $\dot{r} < 0$, the real system has

$$\begin{aligned}\ddot{r} &= u - (1 + \Delta_\alpha)\,\mathrm{sgn}(\dot{r})\alpha\dot{r}^2 \\ &\geq u - (1 - \delta_\alpha)\,\mathrm{sgn}(\dot{r})\alpha\dot{r}^2\end{aligned}$$

so that the real system goes more upward than l_α. Therefore, the trajectory of the actual system goes inward of $\mathscr{D}_\alpha$. □

5.3 Effect of Δ_m

Let l_m denote a state trajectory, starting from the target $r = 0$ with a positive speed $v_0 > 0$ and ending at $r = 0$ and $\dot{r} = v_f$, of a closed-loop system Eq. (3) with the control input $\hat{u}$ with

$$\hat{u} = \begin{cases} -u_{\max} & \text{if } (1+\delta_m)r \geq \dot{r}\left(-\frac{u_{\max}}{K} - c\right) \\ u_{\max} & \text{else if } (1+\delta_m)r < \dot{r}\left(\frac{u_{\max}}{K} - c\right) \\ K\left(c + (1+\delta_m)\frac{r}{\dot{r}}\right) & \text{otherwise} \end{cases} \tag{12}$$

Let $\mathscr{D}_m$ denote a region in the phase plane that is encircled by l_m and $r = 0$, but is outside of the target set $\mathscr{G}$. Then, the following holds.

THEOREM 5.3 (CONVERGENCE WITH UNCERTAIN TTC). *From any states in $\mathscr{D}_m$, the system* Eq. (3) *controlled by the control law* Eq. (9) *will enter $\mathscr{G}$.*

Proof. Again, the proof is based on showing that any states on l_m of the actual system has a direction in the phase plane that goes inward of $\mathscr{D}_m$.

When $r \geq \dot{r}(-\frac{u_{\max}}{K} - c)$, both the real system and the trajectory on l_m have $u = -u_{\max}$, so that the actual system follows l_m.

Otherwise, because $\dot{r} < 0$, the input to the actual system is

$$\begin{aligned}u &= u_{\max}\,\mathrm{sat}\left(\frac{K}{u_{\max}}\left(c + (1+\Delta_m)\frac{r}{\dot{r}}\right)\right) \\ &\geq u_{\max}\,\mathrm{sat}\left(\frac{K}{u_{\max}}\left(c + (1+\delta_m)\frac{r}{\dot{r}}\right)\right)\end{aligned}$$

so that $\ddot{r}$ of the actual system is larger than that of l_m, resulting in a trajectory that goes inward of $\mathscr{D}_m$.

□

5.4 Combined Uncertainties

This subsection combines the effects of the uncertainties discussed above. Consider the following control law

$$u = \begin{cases} (1-\delta_u)\hat{u} & \text{if } \dot{r} \geq 0 \\ (1+\delta_u)\hat{u} & \text{else if } \hat{u} < 0 \\ (1-\delta_u)\hat{u} & \text{otherwise} \end{cases} \tag{13}$$

where $\hat{u}$ is given by Eq. (12). Let l_c denote a state trajectory, starting from the target $r = 0$ with a positive speed $v_0 > 0$ and ending at $r = 0$ and $\dot{r} = v_f$, of a system Eq. (11) controlled by Eq. (13). Let $\mathscr{D}_c$ denote a region in the phase plane that is encircled by l_c and $r = 0$, but is outside of the target set $\mathscr{G}$. Then, the following holds.

THEOREM 5.4 (CONVERGENCE WITH COMBINED UNCERTAINTIES). *From any states in $\mathscr{D}_c$, the system* Eq. (8) *controlled by the control law* Eq. (4) *will enter $\mathscr{G}$.*

The proof is very similar to the ones given above, and is omitted for brevity.

6. NUMERICAL EXAMPLES

This section presents some numerical examples. The following parameters are used.

$$\begin{aligned} u_{\max} &= 0.78 & C_d &= 0.1 \\ \rho &= 1.2041 & A &= 0.09 \\ K &= 1.0 & c &= 2.5 \end{aligned}$$

The target is

$$r_f = 0.1 \qquad v_f = -0.1$$

6.1 Nominal System

The green lines in Figure 5 are the phase plane plot of the closed-loop trajectories from different initial conditions. The blue line shows the boundary $\partial\mathscr{D}$ of the region of attraction. As proven in Section 4, all the trajectories inside this line hits the target.

The time history of those trajectories that reached the target $\mathscr{G}$ are shown in Figure 6.

6.2 Uncertain System

6.2.1 Single Source of Uncertainties

Figure 7 shows the boundaries inside which the system is guaranteed to reach the target $\mathscr{G}$. The black line shows the boundary of the nominal system l; the blue, green, and red lines respectively show the boundary of the uncertain system with one uncertain parameter

$$\begin{aligned} l_u &: & \delta_u &= 0.1 & \delta_\alpha &= 0 & \delta_m &= 0 \\ l_\alpha &: & \delta_u &= 0 & \delta_\alpha &= 0.1 & \delta_m &= 0 \\ l_m &: & \delta_u &= 0 & \delta_\alpha &= 0 & \delta_m &= 0.1. \end{aligned}$$

The same number 0.1 was used for the magnitude of the uncertainty in each plot. Note that in order to account for uncertainties, the region of attraction becomes smaller than that of the nominal system. Also, it can be seen that the green and the black lines are close to each other, showing that this system has small sensitivity to the uncertainty in the drag.

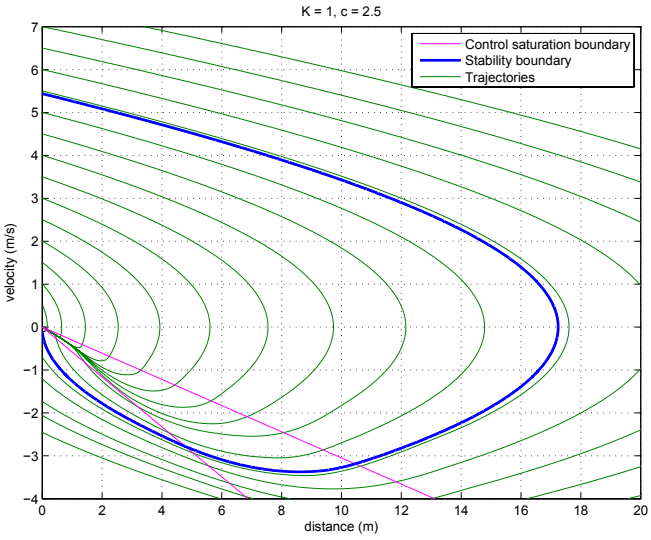

Figure 5. Trajectories in the phase plane

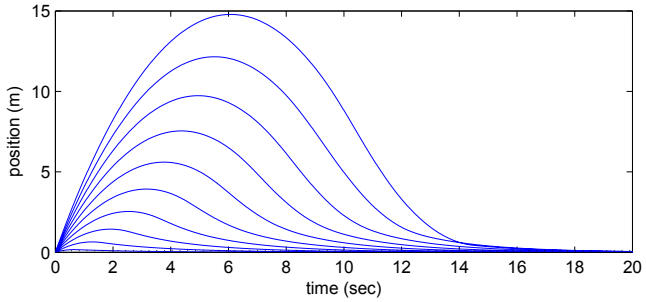

Figure 6. The time history of the trajectories

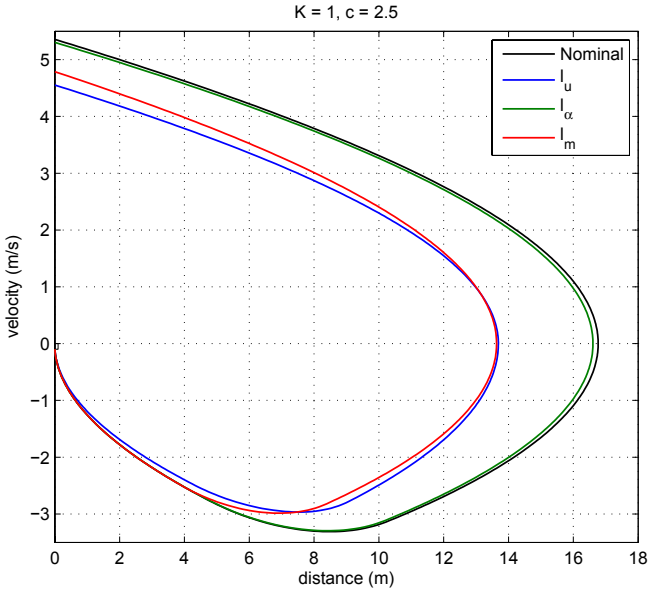

Figure 7. Region of attraction with one uncertain parameter.

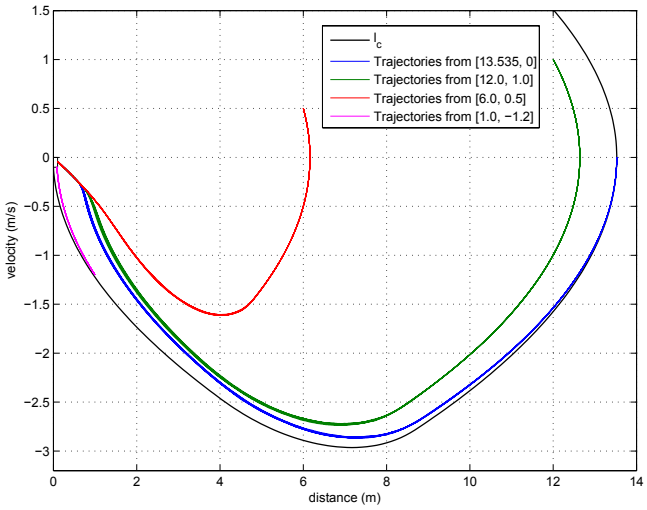

(a) Phase plane plot

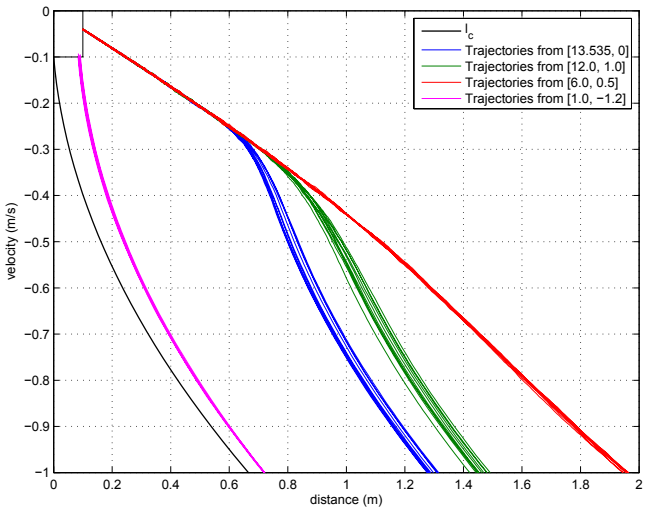

(b) Close-up

Figure 8. Simulation of 10 runs from 4 different initial conditions. The region of attraction l_c is also shown.

6.2.2 Combined Uncertainties

Figure 8 shows the simulation of 10 runs from 4 different initial conditions with

$$\delta_u = 0.05$$
$$\delta_\alpha = 0.1$$
$$\delta_m = 0.05$$

The uncertainty parameters Δ_u, Δ_α, and Δ_m are assumed to be uniformly distributed within the bound. The target region is also shown in Figure 8 with a rectangle.

Note that all the trajectories starting inside l_c successfully reached the target $\mathscr{G}$, despite the existence of the uncertainties. These simulation results confirm the theoretical results presented in Section 5.

7. CONCLUSION

This paper presented an analysis framework of a control law for MAV landing on a target with actuator saturation. The controller is guaranteed to bring the vehicle to the target from a set of initial conditions. The boundary of such initial states is numerically obtained. The results demonstrate that only using the time-to-collision measurement, the vehicle can land at the target with a prespecified tolerance on the impact speed. The numerical simulation showed that the set of allowable initial states is sufficiently large for this approach to be used in the final stage of MAV landing. Future work includes how to select the best set of gains and how the ground effect will affect the overall performance.

Acknowledgment

The authors would like to thank Behcet Ackmissee and Sertac Karaman for the fruitful discussion. The research described in this paper was carried out at the Jet Propulsion Laboratory, California Institute of Technology, and was sponsored by contract # NAS7-03001, task order # NMO71615 through an agreement with the National Aeronautics and Space Administration.

REFERENCES

[1] Office of the Secretary of Defense, "Unmanned aerial systems roadmap," tech. rep. (December 2005).

[2] Srinivasan, M., Zhang, S., Chahl, J., Barth, E., and Venkatesh, S., "How honeybees make grazing landings on flat surfaces," *Biological Cybernetics* **83**, 171–183 (2000).

[3] Lee, D., Davies, M., Green, P., and Weel, F. V. D., "Visual control of velocity of approach by pigeons when landing," *Journal of Experimental Biology* **180**(1), 85–104 (1993).

[4] Hyslop, A. and Humbert, J., "Wide-field integration methods for autonomous navigation in 3-d environments," in [*Proceedings of the AIAA Guidance, Navigation, and Control Conference*], (2008).

[5] Lupton, T. and Sukkarieh, S., "Removing scale biases and ambiguity from 6DoF monocular SLAM using inertial," in [*Proceedings of the IEEE International Conference on Robotics and Automation*], (2008).

[6] Ballard, D. H. and Brown, C. M., [*Computer Vision*], Prentice-Hall (1982).

[7] Gray, R. and Regan, D., "Accuracy of estimating time to collision using binocular and monocular information," *Vision Research* **38**, 499–512 (February 1998).

[8] Lourakis, M. and Orphanoudakis, S., "Using Planar Parallax to Estimate the Time-to-Contact," in [*Proceedings of the IEEE Conference on Computer Vision and Pattern Recognition*], (1999).

[9] Galbraith, J., Kenyon, G., and Ziolkowski, R., "Time-to-Collision Estimation from Motion Based on Primate Visual Processing," *IEEE Transactions on Pattern Analysis and Machine Intelligence* **27**(8), 1279–1291 (2005).

[10] McCarthy, C., Barnes, N., and Mahony, R., "A Robust Docking Strategy for a Mobile Robot Using Flow Field Divergence," *IEEE Transactions on Robotics* **24**(4), 832–842 (2008).

[11] Santos-Victor, J. and Sandini, G., "Visual Behaviors for Docking," *Computer Vision and Image Understanding* **67**(3), 223–238 (1997).

[12] Herisse, B., Russotto, F.-X., Hamel, T., and Mahony, R., "Hovering flight and vertical landing control of a VTOL unmanned aerial vehicle using optical flow," in [*Proceedings of the IEEE/RSJ International Conference on Intelligent Robots and Systems*], (2008).